We are IntechOpen,
the world's leading publisher of
Open Access books
Built by scientists, for scientists

6,900
Open access books available

186,000
International authors and editors

200M
Downloads

Our authors are among the

154
Countries delivered to

TOP 1%
most cited scientists

12.2%
Contributors from top 500 universities

CLARIVATE ANALYTICS
BOOK CITATION INDEX
INDEXED

WEB OF SCIENCE™

Selection of our books indexed in the Book Citation Index
in Web of Science™ Core Collection (BKCI)

Interested in publishing with us?
Contact book.department@intechopen.com

Evaluation of Mitochondrial DNA Dynamics Using Fluorescence Correlation Analysis

Yasutomo Nomura

Department of Systems Life Engineering, Maebashi Institute of Technology,
Japan

1. Introduction

Mitochondria are the sites of oxidative phosphorylation and generate ATP when electron is transferred from respiratory substrates to oxygen by a series of redox reaction in which respiratory enzymes pump protons across the mitochondrial inner membrane from the matrix space[1]. In isolated mitochondria as well as in intact cells, respiration frequently produces reactive oxygen species (ROS). Especially, ROS increased if respiration is perturbed, e.g., ischemia-reperfusion injury [2]. ROS can attack almost all biomolecules unspecifically. In case of DNA, ROS causes single- and double –strand breaks, and base damage[3]. Nevertheless mitochondria metabolize them only partially. Due to the defense system, mitochondrial DNA (mtDNA, ~17 kbp) that mitochondria contain independently of nucleus is particularly vulnerable because it is partially associated with the inner mitochondrial membrane as shown in Fig.(**1A**) [4]. Moreover, mtDNA repair system is weaker than that of nucleus[5]. Since mtDNA codes a part of respiratory enzymes[6], the damages would be harmful to mitochondrial function. On the other hand, because mtDNA forms a complex with proteins and is not naked, a concept that mtDNA have a resistance against ROS is also favored[7]. Therefore, one may need to reconsider mtDNA damage using a newly developed methodology which is able to detect symptoms failed to be found in the previous studies. Among symptoms, the changes in mtDNA dynamics are noticed.

2. mtDNA nucleoid

As shown in Fig.(**1B**), mtDNA molecules are usually clustered within mitochondria as protein-DNA complexes called nucleoid[8]. Cells contain tens to hundreds of nucleoid dependent on the species, growth conditions, differentiation, developmental stage and so on. Each nucleoid contains several mtDNA copies. Among nucleoid proteins reported previously, main proteins were (i) transcription factor A of mitochondria, TFAM[9], (ii) mitochondrial single-stranded DNA binding protein, mtSSB[10], (iii) mtDNA helicase, Twinkle[11], and (iv) mtDNA polymerase, POLG[8]. These proteins would participate in the maintenance of mtDNA. When a cell divides during cell cycle, daughter cells need to receive mtDNA. However, since mtDNA damage probably affects the interaction with nucleoid proteins, transmission of damaged mtDNA may differ from that of intact mtDNA as discussed in heteroplasmy[15]. Indeed, in contrast to neutral polymorphisms, severe mtDNA mutations responsible for diseases in a heteroplasmic state, almost never returned
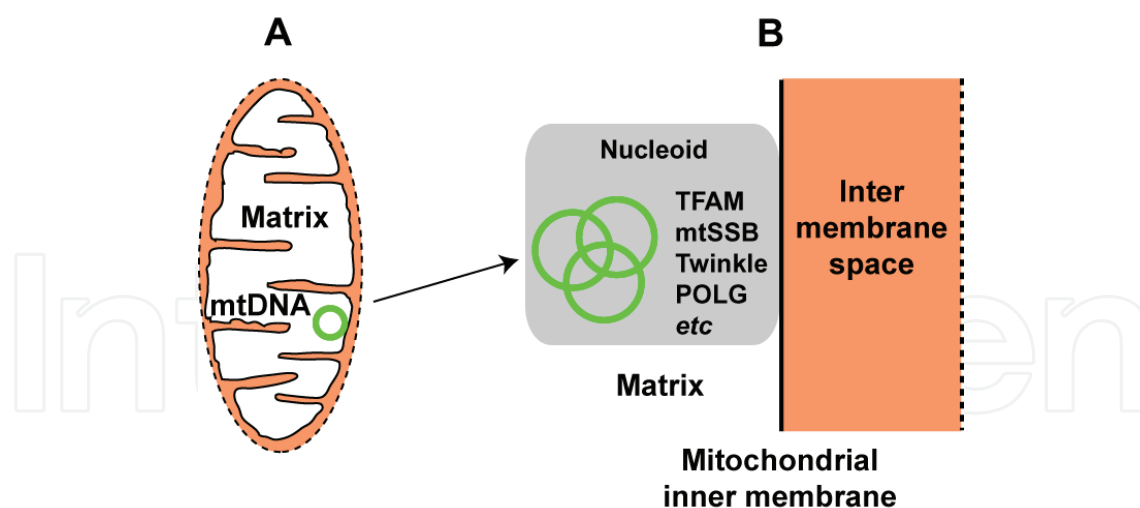
Fig. 1. Structural organization of mitochondrial DNA, mtDNA. (A) Mitochondria have own genetic materials within the matrix. (B) mtDNA nucleoid structure. Several mtDNA molecules within a nucleoid associate to mitochondrial inner membrane through the complex formed with nucleoid proteins such as TFAM, mtSSB, Twinkle, POLG and so on (see text).

to homoplasmy[16]. Large deletions (~5 kb) of mtDNA were very rarely transmitted to the offspring[17]. It was reported that deleterious heteroplasmic mtDNA mutation occurred in early stage of development of primary oocytes from a woman carrying a mtDNA mutation responsible for MELAS, mitochondrial encephalomyopathy with lactic acidosis and stroke-like episodes[18].

Moreover, mitochondria itself are dynamic organelles in post mitotic state as well [12]. When mitochondria move along cytoskeletal tracks, each mitochondrion encounters and undergoes fusion[13]. Consequently, mitochondrial networks spread within an entire cell in some cases. On the other hand, each mitochondrion yields two or more shorter mitochondria when fission occurs[14]. Therefore, in addition to mtDNA damage, mutations in nuclear-encoded genes that play an important role in mitochondria dynamics would also cause changes in mtDNA dynamics. For example, heterozygous mutations in optic atrophy gene 1 product, OPA1, caused autosomal dominant optic atrophy, the most common heritable form of optic neuropathy[19]. Mutations in gene encoding Twinkle or POLG cause the autosomal dominant progressive external opthalmoplegia[11, 20]. Although the organization of nucleoid proteins in fixed cells was revealed by immunocytochemistry, effects of the organization on mtDNA dynamics remained fully unclear. Methods by which mtDNA dynamics can be evaluated would permit to diagnose biopsy samples from patients suspected of having these diseases. Moreover, when we search candidates for compounds that modulate mtDNA dynamics by high throughput screening, image correlation method is one of the useful methods.

3. Direct measurement of mtDNA dynamics

Time-lapse fluorescence microscopy was successfully used to study mtDNA dynamics. When nucleoids were observed in cells that expressed GFP-Twinkle, the average displacement velocity of GFP-Twinkle spots was 0.01 µm/s [21]. However, in this method,

because only a few mtDNAs selected within a cell were analyzed, it is probably hard to determine mtDNA dynamics in a whole cell. In order to analyze mtDNA dynamics in wide area of cytoplasm, image correlation spectroscopy (ICS) are proper because fluorescent particles, namely mtDNAs, are not selected. ICS is an imaging analog of fluorescence correlation spectroscopy (FCS)[22]. Therefore, prior to ICS, principles of FCS are described. In FCS, fluorescent molecules entering a tiny detection area generated by confocal optics emit photons and those exiting the area due to Brownian motion cease to emit them[23, 24]. Based on the fluctuations of fluorescence intensity, the motion of fluorescent molecules is evaluated as diffusion constant. As shown in Fig.(**2**), the fluctuation signal is dependent on molecular weight and the number of molecules.
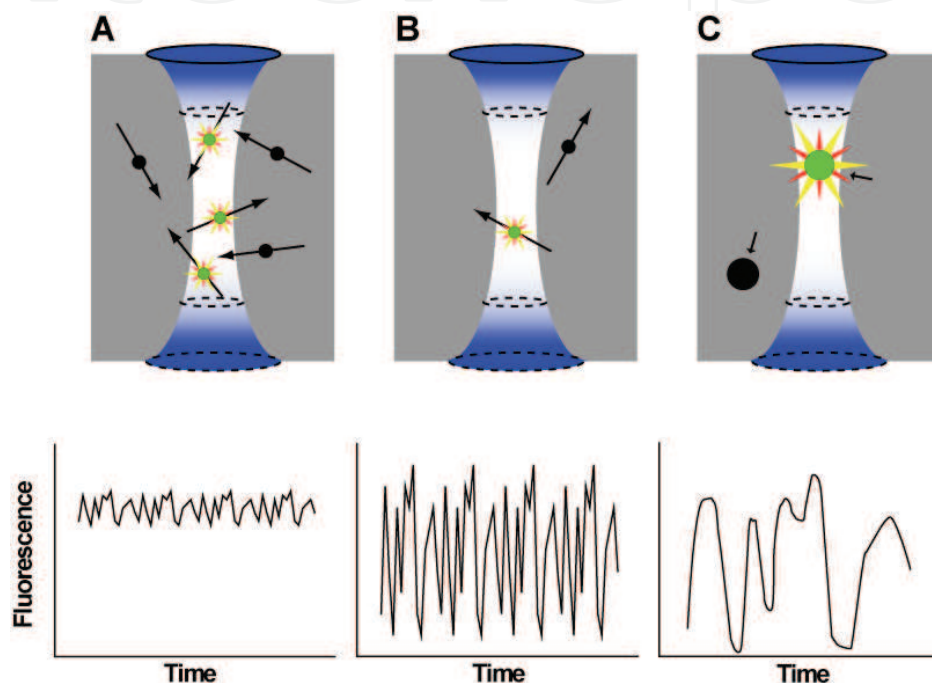
Fig. 2. Effect of molecule number and molecular weight on fluorescence fluctuation. (A) When fluorescent molecules enter and exit tiny detection area (confocal volume element) due to Brownian motion, fluorescence intensity fluctuates. (B) When the fluorescent molecules decrease, the relative fluctuation of fluorescence intensity against the average value increases. (C) When the fluorescent molecules become larger, the fluctuation become slower.

Since fluorescence intensity fluctuates with only a few fluorescent molecules diffusing in and out of the volume element, the intensity at time t, $I(t)$, changes into $I(t+\tau)$, τ seconds later. The normalized autocorrelation function commonly used is calculated from the random fluctuation of fluorescence intensity:

$$G(\tau) = \frac{\langle I(t)I(t+\tau)\rangle}{\langle I(t)\rangle^2} \tag{1}$$

To evaluate the experimentally obtained autocorrelation function, the following analytical expression has been derived [25]:

$$G(\tau) = 1 + \frac{1}{N}\left(1 + \frac{\tau}{\tau_d}\right)^{-1}\left(1 + \frac{s^2\tau}{\tau_d}\right)^{-\frac{1}{2}} \tag{2}$$

In fact, the equation indicates simple diffusion properties, and then represents the time-dependent correlation function for translational diffusion based on fluorescence fluctuation due to Brownian motion of three dimensions, where N is the average number of molecules in the volume element. τ_d is the diffusion time that the molecules take to traverse the detection area in the radial direction. s is the ratio of the axial half-axis to the lateral half-width of the detection area and it can be previously obtained with an authentic material such as rhodamine 6G. When Eq. (2) is fitted to the experimentally obtained autocorrelation function, τ_d and N can be obtained. Although Eq. (2) represents a one-component model for the autocorrelation function, depending on the application, practically, a two-component [26-28] or multicomponent model [29, 30], or even analytical expression for the cross-correlation function [31, 32] is also adopted.
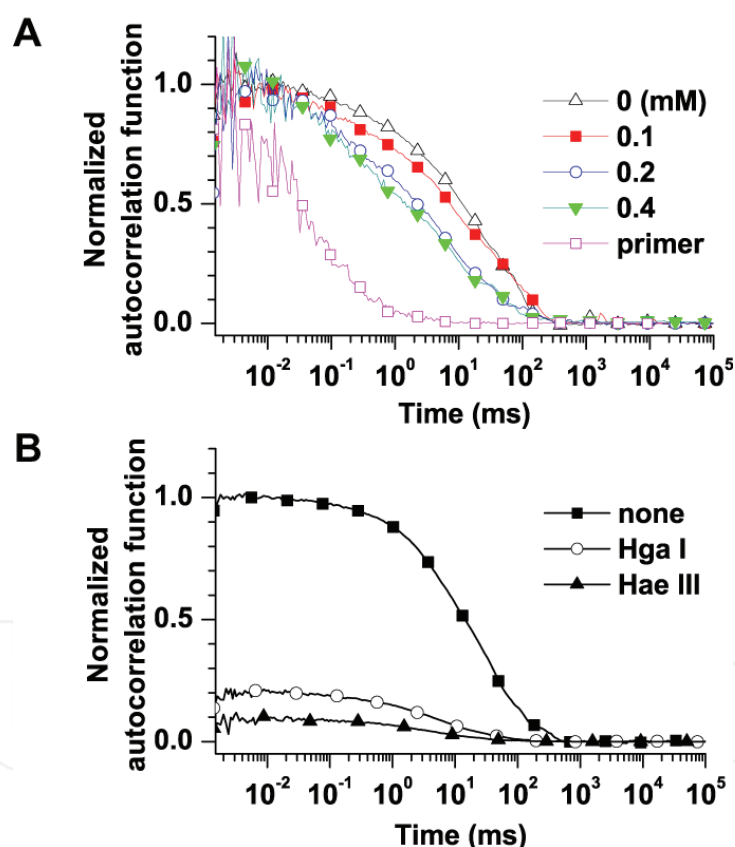

Fig. 3. Fluorescence correlation analysis of mtDNA damage *in vitro*. (A) Changes in normalized autocorrelation functions of long PCR products (~17 kbp) for mtDNA isolated from the cells exposed to H_2O_2 (0 ~ 0.4 mM). For comparison, normalized autocorrelation function of primer is also shown. A decrease in fraction of slow-moving components (long PCR products) shifted normalized autocorrelation function to the left hand side. (B) Effect of restriction digestion on the normalized autocorrelation function of long PCR products for mtDNA. An increase in fluorescent molecules due to the fragmentation resulted in the decrease in amplitude of autocorrelation function.

In order to estimate the vulnerability of mtDNA to oxidative stress, using FCS, the complete mtDNA genome isolated from the cells exposed to H_2O_2 was amplified by long PCR and the product (~17 kbp) was fluorescently labeled with an intercalating dye, YOYO-1 [34]. As shown in Fig.(**3A**), normalized autocorrelation function (normalized ($G(\tau)$-1)) of long PCR for mtDNA product was shifted to the left with the increment of H_2O_2 concentration. When the data were analyzed by a 2-component model, a decrease in the slow component due to mtDNA damage was revealed. In further study, we quantified size distribution of restriction fragments in long PCR product for mtDNA with Hga I and Hae III [30] (Fig.(**3B**)), which indicated changes in molecular number due to fragmentation. Using a multi-component model which was considered as a fragment length-weighted correlation function, we calculated the correlation amplitude expected theoretically and compared it to that measured by FCS (refer [30]). Since these were coincident well, the amplitude measured by FCS would be a very useful index for primary screening for alterations in the entire mitochondrial genome using restriction enzymes that have several polymorphic restriction sites.

4. Image correlation spectroscopy

In ICS which is an imaging analog of FCS, the raw data for image correlation analyses is an image series which is recorded as a function of space and time. The images are usually obtained from a confocal laser scanning microscope (LSM), two-photon LSM or evanescent wave imaging[35]. A generalized spatiotemporal correlation function is defined as:

$$r(\xi,\eta,\tau) = \frac{\left\langle \delta I(x,y,t)\delta I(x+\xi,y+\eta,t+\tau) \right\rangle}{\left\langle I(x,y,t) \right\rangle^2} \tag{3}$$

where a fluctuation in fluorescence, $\delta I(x, y, t)$, is given by:

$$\delta I(x,y,t) = I(x,y,t) - \left\langle I(x,y,t) \right\rangle \tag{4}$$

where $I(x,y,t)$ is the intensity at pixel (x, y) in the image recorded at time t, and $<I(x,y,t)>$ is the average intensity of that image at time t. Every image acquired on a LSM is a convolution of point spread function (PSF) for the microscope with the point-source emission from the fluorophores due to diffraction [36]. This convolution causes the signal from a point-emitter to be spread over a number of pixels. Correlation of fluctuations arising from fluorescent particles within the microscope PSF also confers some critical limitations on ICS approaches. In ICS introduced here, the spatial correlation function is firstly computed and then number of particle is obtained. Next, using the value, when the temporal correlation function is fitted to an analytical model derived from diffusion theory, diffusion coefficient is calculated.

With spatial ICS, a spatial autocorrelation function is calculated from the intensities recorded in the pixels of individual images (Fig.(**4A**)) As shown in the colored surface of Fig.(**4B**), the spatial autocorrelation function of the image is given by Eq. 3 when $\tau = 0$:

$$r(\xi,\eta,0) = \frac{\left\langle \delta I(x,y,t)\delta I(x+\xi,y+\eta,t) \right\rangle}{\left\langle I(x,y,t) \right\rangle^2} \tag{5}$$

where the angular brackets denote spatial averaging over the image, and ξ and η are spatial lag variables corresponding to pixel shifts of the image relative to itself in the x and y directions. The correlation function is then fitted to a 2D Gaussian using a nonlinear least squares algorithm (the grey mesh in Fig.(**4B**)):

$$r(\xi,\eta,0) = g(0,0,0) \cdot \exp\left[-\frac{\xi^2 + \eta^2}{\omega_0^2}\right] + g_\infty \qquad (6)$$

where $g(0,0,0)$ is the zero-lags amplitude, and g_∞ is the long-spatial lag offset to account for an incomplete decay of the correlation function. Fitted parameters are $g(0,0,0)$ and g_∞. In Eq.(6), a Gaussian function is used because the laser beam acts as the spatial correlator and has a Gaussian intensity profile. The zero-lags amplitude of the correlation function is inversely proportional to the number of independent fluorescent particles per beam area. The beam radius of the microscope PSF (ω_0) can be determined using methods such as imaging of fluorescent microspheres with diameter less than diffraction limit [36]. Because the size of ω_0 is wavelength-dependent, the PSF should be measured at excitation wavelength same as the ICS experiment.
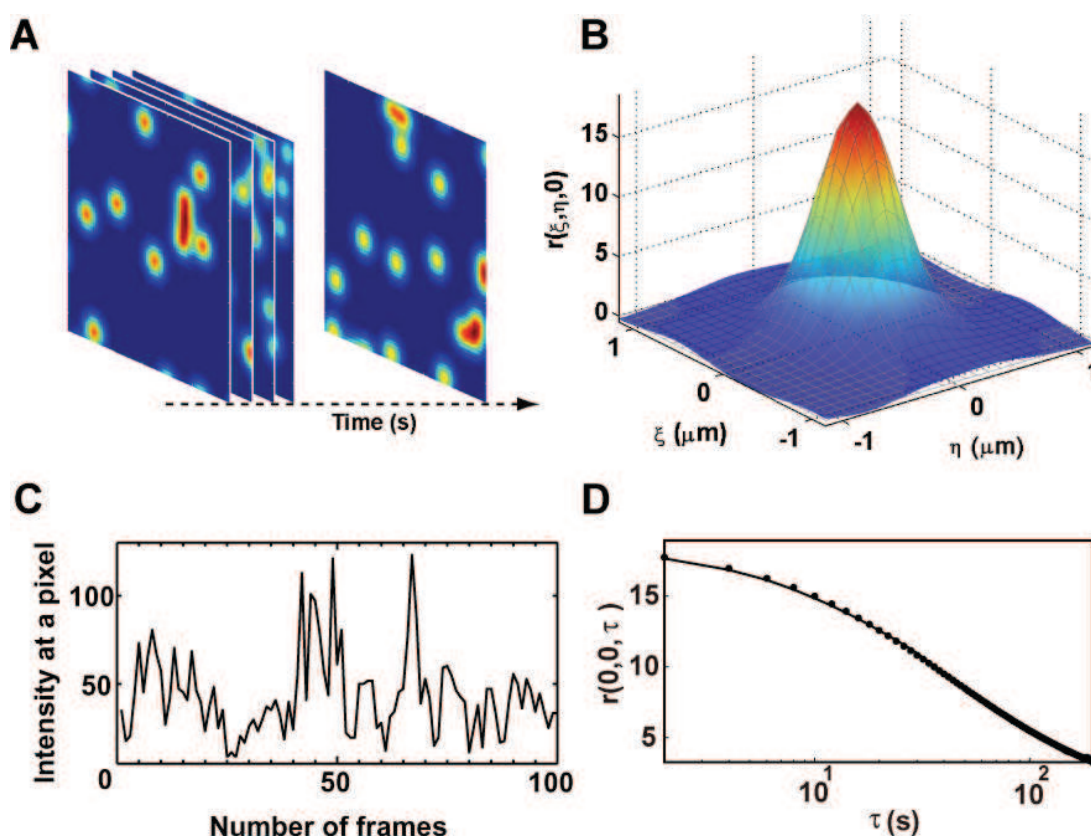

Fig. 4. Image correlation analysis of computer-generated simulations in the case of $\tau_d = 0.001$ $\mu m^2/s$, 0.1 particles/μm^2 and $\omega_0 = 0.4$ μm. (**A**) Temporal image series with 5 $\mu m \times 5$ μm / 2 s. (**B**) The raw correlation function is denoted by the colored surface, and the fitted 2D Gaussian function is denoted by the grey mesh. (**C**) Intensity at a pixel fluctuates with number of frames separated 2 s interval. (**D**) Temporal image correlation function derived from temporal image series (**A**).

Next, as shown in Figs.(**4C** and **D**), temporal autocorrelation function of an image series as a function of time lag τ is obtained from Eq. 3 when ξ and $\eta = 0$:

$$r\left(0,0,\tau\right) = \frac{\left\langle \delta I\left(x,y,t\right)\delta I\left(x,y,t+t\right)\right\rangle}{\left\langle I\left(x,y,t\right)\right\rangle^2} \tag{7}$$

where the angular brackets denote spatial and temporal averaging. Experimentally, τ values are determined by the time between subsequent images in the image series. Depending on the microscope system used, sampling time of image acquisition is usually between 0.03 and 10 s. Here, because it can be assumed that mtDNA in cytoplasm of cells attached strongly on a culture dish behaves as 2D diffusion, the correlation function $r(0,0,\tau)$ was fitted to a simple one component model which was diffusing freely:

$$r\left(0,0,\tau\right) = \frac{g\left(0,0,0\right)}{\left(1+\dfrac{\tau}{\tau_d}\right)} + g_\infty \tag{8}$$

where $g(0,0,0)$ is the zero-lags amplitude dependent on number of fluorescent particles, and g_∞ is the long-time offset. For confocal excitation, the characteristic diffusion time, τ_d is related to the diffusion coefficient, D by:

$$D = \frac{\left\langle \omega_0 \right\rangle^2}{4\tau_d} \tag{9}$$

where ω_0 is e^{-2} radius of the focused beam of the microscope.

5. mtDNA dynamics

Prior to analysis of mtDNA dynamics in living cells, mtDNA localization was determined by cross-correlation analysis of dual-labeled images with specific dyes for mtDNA (PicoGreen [37], PG) and mitochondria (MitoTracker Deep Red, MT) as shown in Fig.(**5A**). The cross-correlation function was calculated by shifting the red image over a distance ξ in the x-direction with respect the green image with $-4 \le \xi \le 4\mu m$ [38]. For each value of ξ, Pearson's correlation coefficient $r_p(\xi)$ was calculated according to:

$$r_p\left(\xi\right) = \frac{\displaystyle\sum_{(x,y)}\left[I_g\left(x,y\right)-\left\langle I_g\right\rangle\right]\left[I_r\left(x+\xi,y\right)-\left\langle I_r\right\rangle\right]}{\sqrt{\displaystyle\sum_{(x,y)}\left[I_g\left(x,y\right)-\left\langle I_g\right\rangle\right]^2}\sqrt{\displaystyle\sum_{(x,y)}\left[I_r\left(x,y\right)-\left\langle I_r\right\rangle\right]^2}} \tag{10}$$

where $I_g(x,y)$ and $I_r(x,y)$ are the intensity of green and red channel at pixel (x,y), and $<I_g>$ and $<I_r>$ are average intensity, respectively. As shown in Fig.(**5B**), the cross-correlation function was obtained by plotting $r_p(\xi)$ against ξ. In principle, a cross-correlation function can be determined for shifts in any direction of the x, y, z-space, but shifts in the x,y-plane are
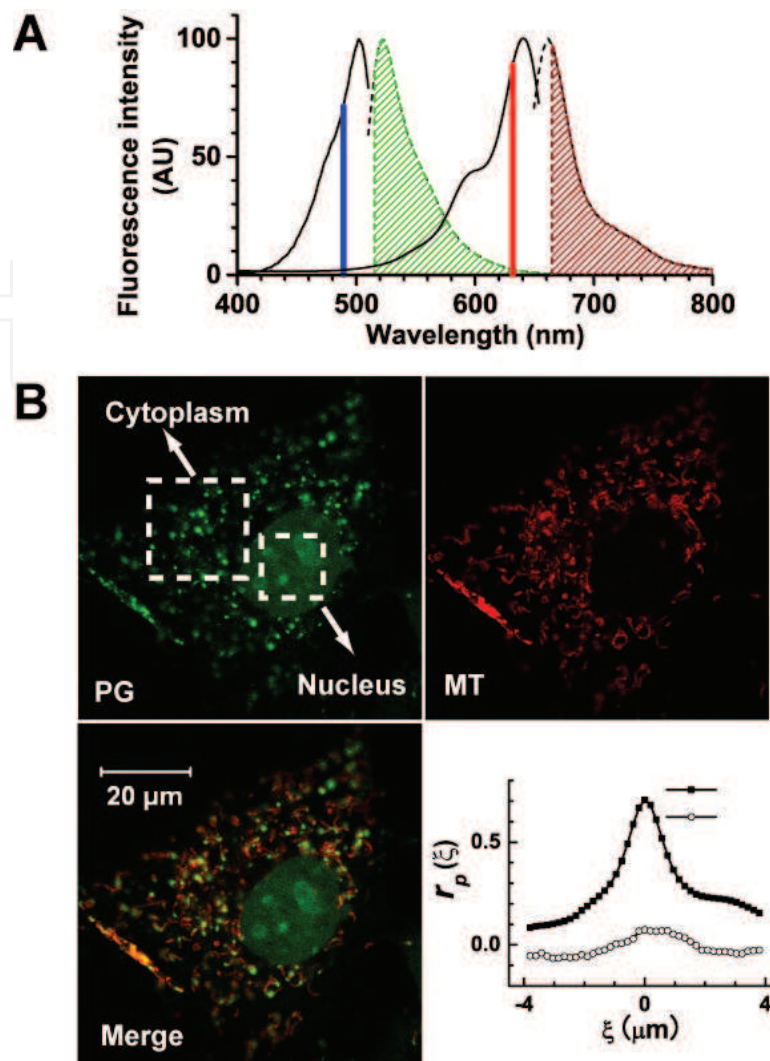
Fig. 5. Localization of mtDNA within mitochondria. (**A**) fluorescence spectra of suspension of cells dual-stained with PicoGreen (ex. 488 nm) for mtDNA and MitoTracker Deep Red (ex. 633 nm) for mitochondria. A solid line shows each excitation spectrum. Using LSM, the hatched area of emission spectra (broken line) was observed. (**B**) Confocal images of mtDNA (PG) and mitochondria (MT) are merged. In right panel, cross-correlation analysis of a dual-labeled image is shown in cytoplasmic (filled squares) and nuclear area (open circles).

preferred because of the limited *z*-resolution of LSM. For simplicity, cross-correlation function for shifts in the *x*-direction was analyzed here. As shown in Fig.(**5B**), in contrast to nucleus, PG signals in cytoplasm was partially localized within mitochondria, as confirmed by $r_p(0)$. Therefore, PG signal would show mtDNA.

As shown in Fig.(**6**), temporal autocorrelation function of mtDNA in living cells could be fitted well using Eq.8. Average of diffusion coefficient of mtDNA was 9.4×10^{-3} μm²/s (25 cells), was stable among 0.2~2 s of sampling time, and was comparable to that of mitochondria (8.2×10^{-3} μm²/s) although graphical data are not shown. Therefore, using sequential frames acquired by a LSM, ICS allowed evaluating both dynamics simultaneously. Diffusion coefficient of mtDNA in single living cells was two digits smaller than that *in vitro* [34], and was comparable to that of mitochondria. This suggests that mtDNA would be bound to an internal structure of mitochondria matrix.
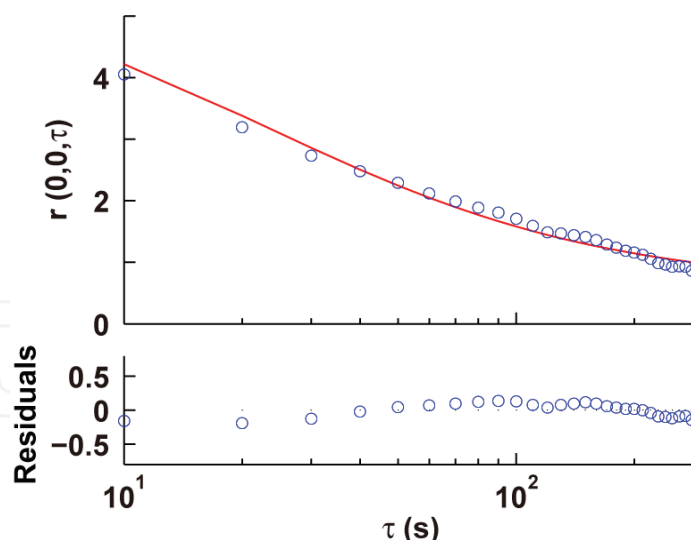
Fig. 6. Typical dynamics of mtDNA analyzed by ICS. In upper panel, temporal image correlation function of raw data (open circles) and fitted analytical model (solid line) are shown. Lower panel is the residuals.

6. Concluding remarks

Because diffusion coefficient depends on molecular weight and/or molecular interaction, diffusion coefficient of mtDNA would allow detecting large deletion of ~5 kb and abnormal transmission. In contrast to recent methods studying mitochondrial genetics such as its RNA expression (e.g., [39]), the present technique is useful for quantifying mtDNA dynamics in single living cells.

7. Acknowledgments

8. References

[1] Santos, J.H.; Hunakova, L.; Chen, Y.; Bortner, C., and Van Houten, B. (2003) *J Biol Chem*, 278(3): 1728.
[2] Das, D.K. and Maulik, N. (2003) *Arch Biochem Biophys*, 420(2): 305.
[3] Demple, B. and Harrison, L. (1994) *Annu Rev Biochem*, 63: 915.
[4] Iborra, F.J.; Kimura, H., and Cook, P.R. (2004) *BMC Biol*, 2: 9.
[5] Yakes, F.M. and Van Houten, B. (1997) *Proc Natl Acad Sci U S A*, 94(2): 514.
[6] Wallace, D.C. (1999) *Science*, 283(5407): 1482.
[7] Spelbrink, J.N. (2010) *IUBMB Life*, 62(1): 19.
[8] Bogenhagen, D.F.; Rousseau, D., and Burke, S. (2008) *J Biol Chem*, 283(6): 3665.
[9] Alam, T.I.; Kanki, T.; Muta, T.; Ukaji, K.; Abe, Y.; Nakayama, H.; Takio, K.; Hamasaki, N., and Kang, D. (2003) *Nucleic Acids Res*, 31(6): 1640.
[10] Maier, D.; Farr, C.L.; Poeck, B.; Alahari, A.; Vogel, M.; Fischer, S.; Kaguni, L.S., and Schneuwly, S. (2001) *Mol Biol Cell*, 12(4): 821.

[11] Spelbrink, J.N.; Li, F.Y.; Tiranti, V.; Nikali, K.; Yuan, Q.P.; Tariq, M.; Wanrooij, S.; Garrido, N.; Comi, G.; Morandi, L.; Santoro, L.; Toscano, A.; Fabrizi, G.M.; Somer, H.; Croxen, R.; Beeson, D.; Poulton, J.; Suomalainen, A.; Jacobs, H.T.; Zeviani, M., and Larsson, C. (2001) *Nat Genet*, 28(3): 223.

[12] Liesa, M.; Palacin, M., and Zorzano, A. (2009) *Physiol Rev*, 89(3): 799.

[13] Detmer, S.A. and Chan, D.C. (2007) *Nat Rev Mol Cell Biol*, 8(11): 870.

[14] Berman, S.B.; Pineda, F.J., and Hardwick, J.M. (2008) *Cell Death Differ*, 15(7): 1147.

[15] Malka, F.; Lombes, A., and Rojo, M. (2006) *Biochim Biophys Acta*, 1763(5-6): 463.

[16] Chinnery, P.F.; Thorburn, D.R.; Samuels, D.C.; White, S.L.; Dahl, H.M.; Turnbull, D.M.; Lightowlers, R.N., and Howell, N. (2000) *Trends Genet*, 16(11): 500.

[17] Chinnery, P.F.; DiMauro, S.; Shanske, S.; Schon, E.A.; Zeviani, M.; Mariotti, C.; Carrara, F.; Lombes, A.; Laforet, P.; Ogier, H.; Jaksch, M.; Lochmuller, H.; Horvath, R.; Deschauer, M.; Thorburn, D.R.; Bindoff, L.A.; Poulton, J.; Taylor, R.W.; Matthews, J.N., and Turnbull, D.M. (2004) *Lancet*, 364(9434): 592.

[18] Brown, D.T.; Samuels, D.C.; Michael, E.M.; Turnbull, D.M., and Chinnery, P.F. (2001) *Am J Hum Genet*, 68(2): 533.

[19] Alexander, C.; Votruba, M.; Pesch, U.E.; Thiselton, D.L.; Mayer, S.; Moore, A.; Rodriguez, M.; Kellner, U.; Leo-Kottler, B.; Auburger, G.; Bhattacharya, S.S., and Wissinger, B. (2000) *Nat Genet*, 26(2): 211.

[20] Van Goethem, G.; Dermaut, B.; Lofgren, A.; Martin, J.J., and Van Broeckhoven, C. (2001) *Nat Genet*, 28(3): 211.

[21] Garrido, N.; Griparic, L.; Jokitalo, E.; Wartiovaara, J.; van der Bliek, A.M., and Spelbrink, J.N. (2003) *Mol Biol Cell*, 14(4): 1583.

[22] Wiseman, P.W.; Brown, C.M.; Webb, D.J.; Hebert, B.; Johnson, N.L.; Squier, J.A.; Ellisman, M.H., and Horwitz, A.F. (2004) *J Cell Sci*, 117(Pt 23): 5521.

[23] Nomura, Y.; Nakamura, T.; Feng, Z., and Kinjo, M. (2007) *Curr Pharm Biotechnol*, 8(5): 286.

[24] Rigler, R.; Mets, U.; Widengren, J., and Kask, P. (1993) *Eur. Biopys. J.* , 22: 166.

[25] Maiti, S.; Haupts, U., and Webb, W.W. (1997) *Proc Natl Acad Sci U S A*, 94(22): 11753.

[26] Kinjo, M. and Rigler, R. (1995) *Nucleic Acids Res*, 23(10): 1795.

[27] Saito, K.; Ito, E.; Takakuwa, Y.; Tamura, M., and Kinjo, M. (2003) *FEBS Lett*, 541(1-3): 126.

[28] Walter, N.G.; Schwille, P., and Eigen, M. (1996) *Proc Natl Acad Sci U S A*, 93(23): 12805.

[29] Kinjo, M.; Nishimura, G.; Koyama, T.; Mets, and Rigler, R. (1998) *Anal Biochem*,

[30] Nomura, Y.; Fuchigami, H.; Kii, H.; Feng, Z.; Nakamura, T., and Kinjo, M. (2006) *Exp Mol Pathol*, 80(3): 275.

[31] Eigen, M. and Rigler, R. (1994) *Proc Natl Acad Sci U S A*, 91(13): 5740.

[32] Saito, K.; Wada, I.; Tamura, M., and Kinjo, M. (2004) *Biochem Biophys Res Commun*, 324(2): 849.

[33] Driggers, W.J.; LeDoux, S.P., and Wilson, G.L. (1993) *J Biol Chem*, 268(29): 22042.

[34] Nomura, Y.; Fuchigami, H.; Kii, H.; Feng, Z.; Nakamura, T., and Kinjo, M. (2006) *Anal Biochem*, 350(2): 196.

[35] Kolin, D.L. and Wiseman, P.W. (2007) *Cell Biochem Biophys*, 49(3): 141.

[36] Yoo, H.; Song, I., and Gweon, D.G. (2006) *J Microsc*, 221(Pt 3): 172.

[37] Ashley, N.; Harris, D., and Poulton, J. (2005) *Exp Cell Res*, 303(2): 432.

[38] van Steensel, B.; van Binnendijk, E.P.; Hornsby, C.D.; van der Voort, H.T.; Krozowski, Z.S.; de Kloet, E.R., and van Driel, R. (1996) *J Cell Sci*, 109 (Pt 4): 787.

[39] Ozawa, T.; Natori, Y.; Sato, M., and Umezawa, Y. (2007) *Nat Methods*, 4(5): 413.
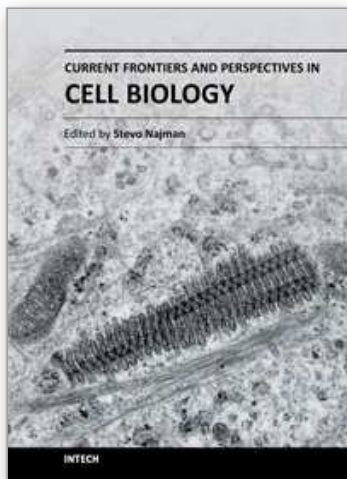
Current Frontiers and Perspectives in Cell Biology

Edited by Prof. Stevo Najman

How to reference

In order to correctly reference this scholarly work, feel free to copy and paste the following:

INTECH
open science | open minds